Received: 28 May 2019 | Accepted: 13 January 2020

DOI: 10.1002/jcp.29606

ORIGINAL RESEARCH ARTICLE

Journal of Cellular Physiology WILEY

Omega-3 and Omega-6 polyunsaturated fatty acids stimulate vascular differentiation of mouse embryonic stem cells

Amer Taha[1] | Fatemeh Sharifpanah[1] | Maria Wartenberg[2] | Heinrich Sauer[1]

[1]Department of Physiology, Justus Liebig University Giessen, Giessen, Germany

[2]Department of Cardiology, Clinic of Internal Medicine I, University Heart Center, Jena University Hospital, Jena, Germany

Correspondence
Heinrich Sauer, Department of Physiology, Justus Liebig University Giessen, Aulweg 129, 35392 Giessen, Germany.
Email: heinrich.sauer@physiologie.med.uni-giessen.de

Funding information
Better German Academic Exchange Service; RB Bretzel Foundation

Abstract

Polyunsaturated fatty acids (PUFAs) and their metabolites may influence cell fate regulation. Herein, we investigated the effects of linoleic acid (LA) as ω-6 PUFA, eicosapentaenoic acid (EPA) as ω-3 PUFA and palmitic acid (PA) on vasculogenesis of embryonic stem (ES) cells. LA and EPA increased vascular structure formation and protein expression of the endothelial-specific markers fetal liver kinase-1, CD31 as well as VE-cadherin, whereas PA was without effect. LA and EPA increased reactive oxygen species (ROS) and nitric oxide (NO), activated endothelial NO synthase (eNOS) and raised intracellular calcium. The calcium response was inhibited by the intracellular calcium chelator BAPTA, sulfo-N-succinimidyl oleate which is an antagonist of CD36, the scavenger receptor for fatty acid uptake as well as by a CD36 blocking antibody. Prevention of ROS generation by radical scavengers or the NADPH oxidase inhibitor VAS2870 and inhibition of eNOS by L-NAME blunted vasculogenesis. PUFAs stimulated AMP activated protein kinase-α (AMPK-α) as well as peroxisome proliferator-activated receptor-α (PPAR-α). AMPK activation was abolished by calcium chelation as well as inhibition of ROS and NO generation. Moreover, PUFA-induced vasculogenesis was blunted by the PPAR-α inhibitor GW6471. In conclusion, ω-3 and ω-6 PUFAs stimulate vascular differentiation of ES cells via mechanisms involving calcium, ROS and NO, which regulate function of the energy sensors AMPK and PPAR-α and determine the metabolic signature of vascular cell differentiation.

KEYWORDS
embryonic stem cells, nitric oxide, polyunsaturated fatty acids, reactive oxygen species, vasculogenesis

1 | INTRODUCTION

Recently an American Heart Association presidential advisory on dietary fats and cardiovascular disease (CVD) discussed and suggested that lower intake of saturated fat and higher intake of polyunsaturated and monounsaturated fat is associated with lower rates of CVD and cardiovascular mortality (Rimm et al., 2018). In contrast, a recent analysis of published clinical trials suggested that increasing eicosapentaenoic acid (EPA) and docosahexaenoic acid (DHA) has little or no effect on mortality or cardiovascular health (Abdelhamid et al., 2018). The main beneficial health effects have been mainly attributed to ω-3 and ω-6 polyunsaturated fatty acids (PUFAs). α-linolenic acid (ALA, 18:3, n-3) is found in plant oils, EPA (20:5, n-3), and DHA (22:6, n-3) are originating in marine algae and

phytoplankton as well as in the ascending food chain in marine crustaceans and marine fish. The lead substance for ω-6 PUFAs is LA (18:2, n-6), which is produced in many nuts and seeds and is a precursor of arachidonic acid (AA; Sokola-Wysoczanska et al., 2018). Mammals are unable to produce ω-3 fatty acids, but can ingest the shorter-chain ω-3 fatty acid ALA through diet and use it to synthetize the essential ω-3 PUFAs EPA and DHA. After uptake into cells, PUFAs are metabolized by cyclooxygenases, lipoxygenases, and cytochrome P450 enzymes (CYP) to generate bioactive eicosanoids, including prostanoids, leukotrienes, hydroxyeicosatetraenoic acids, and epoxyeicosatrienoic acids (Hu, Fromel, & Fleming, 2018). CYP enzymes are membrane-bound, heme-containing terminal oxidases that are part of a multi-enzyme complex, which also includes a FAD/FMN-containing NADPH cytochrome P450 reductase and cytochrome b5 (Hu et al., 2018). The effect of ω-3 and ω-6 PUFAs on vasculogenic and angiogenic processes remains controversial. It has been suggested that ω-6 PUFAs and their metabolites initiate inflammatory signaling pathways downstream of arachidonic acid and promote angiogenesis by increasing growth factor expression (Innes & Calder, 2018), whereas ω-3 PUFAs have anti-inflammatory, antiangiogenic, and antitumor properties (Kang & Liu, 2013). The antiangiogenic effect of ω-3 PUFAs, that is, EPA has been attributed to inhibition of endothelial cell migration (Tsuzuki, Shibata, Kawakami, Nakagawa, & Miyazawa, 2007) and tube formation (Kanayasu et al., 1991), and by depression of angiogenic growth factors (Spencer et al., 2009). However, a recent study has shown that ω-3 PUFAs can promote angiogenesis in placenta-derived mesenchymal stromal cells (Mathew & Bhonde, 2018). Moreover, fish oil-enriched diet protected against ischemia by improving angiogenesis, endothelial progenitor cell (EPC) function and postnatal neovascularization (Turgeon et al., 2013). These data were confirmed in a human setting showing that postprandial hyperglycemia and ω-3 PUFAs contribute to EPC recruitment in patients with coronary artery disease (Morishita et al., 2016). The HMG-CoA-reductase inhibitor rosuvastatin or its combination with ω-3 fatty acids increased circulating $CD34^+$ progenitor cells and enhanced endothelial cell colony formation (Chantzichristos et al., 2016). A diet rich in fish oils promoted hematopoiesis in the bone marrow and spleen of mice (Xia et al., 2015). Taken together these data suggest that ω-3 PUFAs may exert antiangiogenic effects in the mature vascular bed but may be proangiogenic in endothelial progenitor cell or stem cell settings. This may be due to a metabolic signature which is different in stem cells and progenitor cells as compared with terminally differentiated cells (Cha et al., 2017), and may be regulated by the energy sensors AMP activated protein kinase (AMPK) and peroxisome proliferator-activated receptor α (PPAR-α).

In the present study, we investigated vasculogenesis of mouse embryonic stem (ES) cells exposed to either EPA as ω-3 PUFA, LA as ω-6 PUFA and PA as unsaturated fatty acid. Our data demonstrate that EPA as well as LA increased vasculogenesis by mechanisms involving reactive oxygen species (ROS), nitric oxide (NO), and changes in intracellular calcium, which are locked to the energy sensors AMPK and PPAR-α.

2 | MATERIALS AND METHODS

2.1 | Cultivation of ES cells and embryoid body formation

Cultivation of ES cells and formation of embryoid bodies was performed as previously described (Ali, Sharifpanah, Wartenberg, & Sauer, 2018). Briefly, mouse ES cells (line CCE) were cultivated on mitotically inactivated feeder layers of primary mouse embryonic fibroblasts (purchased from Amsbio, Abingdon, UK.) in Iscove's basal medium (cat. no. F0465; Biochrom, Berlin, Germany). The cell culture medium was supplemented with 15% heat-inactivated (56°C, 30 min) fetal calf serum (FCS; cat. no. F7524; Sigma-Aldrich, Taufkirchen, Germany), 2 mM glutamine, (cat. no. M11-004; PAA, Cölbe, Germany), 100 μM 2-mercaptoethanol (cat no. M6250; Sigma-Aldrich), 1% (vol/vol) NEA non-essential amino acids stock solution (cat. no. M7145; Biochrom), 1 mM Na^+-pyruvate (cat. no. L0473; Biochrom), 0.4% penicillin/streptomycin (cat. no. A2212; Biochrom) and 1,000 U/ml leukemia inhibitory factor (LIF; cat. no. LIF1010; Merck-Millipore, Darmstadt, Germany) in a humidified environment containing 5% CO_2 at 37°C. Cell cultures were passaged every 2–3 days. Adherent cells were enzymatically dissociated to form three-dimensional embryoid body tissue using 0.05% trypsin-EDTA in phosphate-buffered saline (PBS; cat. no. R001100; Thermo-Fisher Scientific, Waltham, MA). After dissociation, single cells were seeded at a density of 3×10^6 cells/ml in 250 ml siliconized spinner flasks (cat. no. 182 051; CellSpin, Integra Biosciences, Zizers, Switzerland) containing 125 ml Iscove's medium supplemented as described above, but in the absence of LIF. After 24 hr, 125 ml medium was added to give a final volume of 250 ml. The spinner flask medium was stirred at 20 rpm. using a stirrer system (Integra Biosciences). The spinning direction was changed every 1440°. A volume of 125 ml cell culture medium was exchanged every day.

2.2 | Immunohistochemistry

Immunohistochemistry was performed as described previously (Ali et al., 2018). In brief, monoclonal rat anti-mouse platelet endothelial cell adhesion molecule-1 (PECAM-1/CD31; cat. no. CBL1337; Merk-Millipore; dilution 1:100) was used as primary antibody. The embryoid bodies were fixed in ice-cold methanol for 20 min at −20°C, and washed with PBS containing 0.01% Triton X-100 (PBST). Blocking against unspecific binding was performed for 60 min at room temperature with 10% fat-free milk powder (cat. no. A0830; AppliChem, Darmstadt, Germany) dissolved in PBST. Embryoid bodies were subsequently incubated overnight at 4°C with primary antibody (dilution 1:100) dissolved in PBST supplemented with 10% fat-free milk powder. The embryoid bodies were thereafter washed three times with PBST and re-incubated for 1 hr at room temperature in the dark with Alexa Fluor 488-conjugated donkey anti-rat immunoglobulin G (IgG) secondary antibody (cat. no. 712-546-153; Jackson ImmunoResearch Laboratories, Cambridgeshire, UK) diluted 1:100 in PBST containing 10% fat-free milk powder. After washing

three times with PBST, the tissues were stored in PBST until inspection.

2.3 | Quantification of vasculogenesis in embryoid bodies

The quantification of vasculogenesis in embryoid bodies was performed as previously described (Ali et al., 2018). Fluorescence recordings were performed by means of a confocal laser scanning setup (Leica SP2 AOBS, Leica, Wetzlar, Germany) connected to an inverted microscope. The confocal setup was equipped with a 5 mW helium/neon laser, single excitation 633 nm, and an argon–ion laser, single excitation 488 nm. Emission was recorded using the band-pass filter BP 515-550 and long-pass LP 650 filter sets, respectively. For the analysis a 10×, NA 0.5 objective was used. The pinhole settings of the confocal setup were adjusted to give a full-width half maximum of 5 µm. For the quantification of capillary areas within embryoid bodies an optical sectioning routine based on confocal laser scanning microscopy was used. Images (512 × 512 pixels) were acquired from CD31-stained embryoid bodies using the extended depth of focus algorithm of the confocal setup. In brief, 10 full frame images, separated by a distance of 10 µm in z-direction, were recorded. The obtained images included information of the capillary area and spatial organization of CD31-positive cell structures in a tissue slice 100 µm thick. The acquired images were processed to generate a single in-focus image projection of vascular structures in the scanned tissue slice. By use of the image analysis software Metamorph (Molecular Devices, San José, C.A.), the branching points of vascular structures within the three-dimensional projection were identified and counted in relation to the size of the respective embryoid body.

2.4 | Western blot analysis

Protein expression was assessed by western blot technique following a previously published protocol (Ali et al., 2018). Briefly, protein extraction was carried out after washing the embryoid bodies in PBS and lysing in radioimmunoprecipitation assay lysis buffer (50 mM Tris-HCl [pH 7.5], 150 mM NaCl, 1 mM EDTA (pH 8.0), 1 mM glycerophosphate, 0.1% sodium dodecyl sulfate, 1% Nonidet P-40) supplemented with protease inhibitor cocktail (cat. no. K271-500; BioVision, Milpitas Blvd, Milpitas) and phosphatase inhibitor cocktail (cat. no. P0044; Sigma-Aldrich) for 20 min on ice. To pellet the debris, samples were centrifuged at 25,000*g* for 10 min at 4°C. After determination of the protein concentration using a Lowry protein assay, 20 µg of protein samples were boiled for 10 min at 70°C and separated in PAGEr Ex Precast (4–12%) mini gels (cat. no. 59722; Lonza, Cologne, Germany). Subsequently they were transferred to polyvinylidene difluoride membranes by the XCell SureLock Mini-Cell Blot Module (Thermo-Fisher Scientific) at 20 V for 90 min. Membranes were blocked with 5% (wt/vol) dry fat-free milk powder in Tris-buffered saline with 0.1% Tween (TBST) for 60 min at room temperature. Incubation with primary antibody was done at 4°C overnight. Used primary antibodies were: Rat anti-mouse VE-cadherin (dilution 1:1,000; cat. no. 555289; BD Biosciences, Heidelberg, Germany), rabbit anti-mouse fetal liver kinase-1 (FLK-1; dilution 1:1,000; cat. no. 9698; Cell Signaling Technology, Frankfurt, Germany), goat anti-mouse CD31 (dilution 1:100; cat. no. 910003; BioLegend, Koblenz, Germany), rabbit anti-mouse GAPDH (dilution 1:1,000) (cat. no. ab9485; Abcam, Cambridge, UK), rabbit anti-mouse β-actin (dilution 1:1,000) (cat. no. 622102; BioLegend), mouse anti-vinculin (dilution 1:200; cat. no. V9131; Sigma-Aldrich), rabbit anti-mouse phospho-endothelial NO synthase (p-eNOS; Ser1177; dilution 1:1,000; cat. no. 9571S; Cell Signaling Technology), rabbit anti-mouse phospho-AMPK-α (Thr172; dilution 1:1,000; cat. no. 25352535 S; Cell Signaling Technology), rabbit anti-mouse phospho-PPAR-α (S12; dilution 1:1,000; cat. no. ab3484; Abcam). After washing with 0.1% TBST, the membrane was incubated with a horseradish peroxidase (HRP)-conjugated secondary antibody (dilution 1:1,000; donkey anti-rabbit IgG [HRP]; cat. no. ab205722; Abcam), donkey anti-goat IgG (cat. no. PAB10570; Abnova, Heidelberg, Germany), donkey anti-rat IgG (HRP; cat. no. ab102265; Abcam), (horse anti-mouse IgG (HRP; cat. no. #7076; Cell Signaling Technology) for 60 min at room temperature. The blot was developed using enhanced chemiluminescent detection to produce a chemiluminescence signal. For quantification, the density of protein bands on the western blot image, which was acquired using the peqlab gel documentation system (VWR, Darmstadt, Germany), was assessed by ImageJ. The final quantification reflects the relative amounts of protein as a ratio of each target protein band to the respective housekeeping protein.

2.5 | Measurement of ROS generation

Intracellular ROS levels were measured as described by (Bartsch et al., 2011) using the fluorescent dye 2′7′-dichlorodihydrofluorescein diacetate (H_2DCF-DA; cat. no. D399; Thermo-Fisher Scientific), which is a nonpolar compound that is converted into a nonfluorescent polar derivative (H_2DCF) by cellular esterases after incorporation into cells. H_2DCF is membrane impermeable and is rapidly oxidized to the highly fluorescent 2′7′-dichlorofluorescein (DCF) in the presence of intracellular ROS. For the experiments, embryoid bodies (Day 5 of differentiation) were incubated in serum-free medium, and H_2DCF-DA (20 µM) dissolved in dimethyl sulfoxide was added. After 30 min, intracellular DCF fluorescence (corrected for background fluorescence) was evaluated in 3,600 µm² regions of interest using an overlay mask. For fluorescence excitation, the 488 nm argon–ion laser band of the confocal laser scanning microscope was used. Emission was recorded at an emission band of 515–550 nm.

2.6 | Measurement of NO generation

NO generation was evaluated as described (Mascheck, Sharifpanah, Tsang, Wartenberg, & Sauer,2015; Sharifpanah, Ali, Wartenberg, & Sauer, 2019) by use of the cell permeable specific fluorescent NO indicator DAF-FM (cat. no. D23844; Thermo-Fisher Scientific). After incorporation

into cells, DAF-FM is converted via a NO-specific mechanism to an intensely fluorescent triazole derivative. Embryoid bodies (Day 5 of differentiation) were incubated for 30 min in cell culture medium with DAF-FM (10 μM). Subsequently, embryoid bodies were washed with serum-free medium, and cells were incubated for further 30 min in a CO_2 incubator. They were finally transferred to an incubation chamber mounted to the inspection table of the confocal setup, and DAF fluorescence was recorded in single embryoid bodies using the 488 nm line of the argon–ion laser of the confocal setup and emission >515 nm.

2.7 | Recording of intracellular calcium concentrations

Intracellular calcium was recorded in single cells as described (Mascheck et al., 2015). Single cell preparations were obtained by enzymatic digestion of 3-day-old embryoid bodies for 30 min at 37°C in PBS containing 2 mg/ml collagenase B (cat. no. 11088815001; Roche Diagnostics, Mannheim, Germany). Dissociated single cells were plated onto gelatin-coated cover slips in 24-well cell culture plates (Greiner Bio-One, Frickenhausen, Germany), and cultivated in Iscove's medium supplemented with 15% FCS. Following 24 hr of culture, cells were loaded in serum-free medium with 5 μM Fluo-4/AM (cat. no. F14201; Thermo-Fisher Scientific) for 30 min. Subsequently, the cover slips were transferred in fresh serum-free cell culture medium to the incubation chamber of the confocal laser scanning microscope Leica SP2, AOBS. Fluorescence excitation was performed at 488 nm, emission was recorded at 500–550 nm. Sampling rate was 2 frames/s. The fluorescence emission of single cells was assessed by using the image analysis software of confocal setup.

2.8 | Statistical analysis

For statistical analysis PRISM statistics software (GraphPad Software, San Diego, CA) was used. Data are given as mean ± standard deviation, with *n* denoting the number of experiments performed with independent ES cell cultures. In each experiment at least 20 culture objects were analyzed unless otherwise indicated. Student's *t* test for unpaired data and one-way ANOVA were applied as appropriate for statistical analysis. A value of $p < .05$ (*) or ($^{\#}$) was considered significant.

3 | RESULTS

3.1 | Stimulation of vasculogenesis by EPA and LA

To evaluate the effect of PUFAs on vasculogenesis, embryoid bodies were incubated with either EPA or LA in concentrations ranging from 1 to 100 μM and vascular structure formation as well as protein expression of the vascular markers PECAM-1 and VE-cadherin were investigated. EPA as well as LA treatment dose-dependent significantly increased vascular structure formation (Figure 1a–c) and the expression of vascular markers (Figure 1e–h). In contrast, treatment with PA (10, 50, 100 μM) did not affect vasculogenesis as compared with the untreated and the vehicle control (Figure 1d). Optimum effects on vasculogenesis were achieved with 10–50 μM EPA and LA. Moreover, increased expression of FLK-1 which is an early marker of vascular progenitor cells, was observed upon either EPA or LA treatment (Figure 1i,j), suggesting stimulation of vasculogenesis in ES cells upon incubation with PUFAs.

3.2 | Generation of ROS and NO upon treatment of ES cells with PUFAs

Previous studies of us and others have demonstrated that cardiovascular differentiation of ES cells is dependent on ROS and NO, acting as signaling molecules in intracellular signal transduction pathways (Ali et al., 2018; Cencioni et al., 2018; Sharifpanah, Behr, Wartenberg, & Sauer, 2016). We therefore assessed ROS generation using the ROS-sensitive indicator H_2DCF-DA as well as the NO-sensitive indicator DAF-FM for ROS and NO determination, respectively. Moreover, activation of eNOS was evaluated upon treatment with either EPA or LA. It was observed that treatment with EPA and LA (10 and 50 μM) increased ROS generation (Figure 2a,b). Investigation of the time course of ROS generation by LA revealed that ROS production occurred within few min after PUFA administration and remained on an elevated plateau for at least 24 hr (Figure 2c). Coadministration of EPA and LA with the free radical scavengers Trolox (100 μM) and NMPG (100 μM) completely abolished the stimulation of vascular structure formation obtained upon PUFA treatment (Figure 2d–f). Moreover, the stimulation of vasculogenesis by PUFAs was significantly inhibited in presence of the NADPH oxidase inhibitor VAS2870 (50 μM; Figure 2d–f). PUFA treatment of differentiating ES cells likewise increased NO generation (Figure 3a–c) and increased eNOS phosphorylation at residue Ser1177 within few min (Figure 3d,e). The phosphorylation of eNOS as well as vascular structure formation were completely blunted in presence of the NOS inhibitor L-NAME (Figure 3f,g), indicating the importance of NO in parallel to ROS for the induction of vasculogenesis by PUFAs.

3.3 | Release of intracellular calcium upon PUFA treatment

ω-3 as well as ω-6 PUFAs have been previously shown to raise intracellular calcium in different cells (Carrillo et al., 2011; Kim et al., 2015; Mobraten et al., 2013). To investigate whether changes in intracellular calcium concentrations relay PUFA treatment to the cellular messengers ROS and NO as well as to vasculogenesis of ES cells, we assessed intracellular calcium changes by Fluo-4 microfluorometry. It was evidenced that both EPA and LA (50 μM) treatment transiently raised intracellular calcium concentrations (Figures 4aii,viii). Pretreatment for 30 min with the intracellular

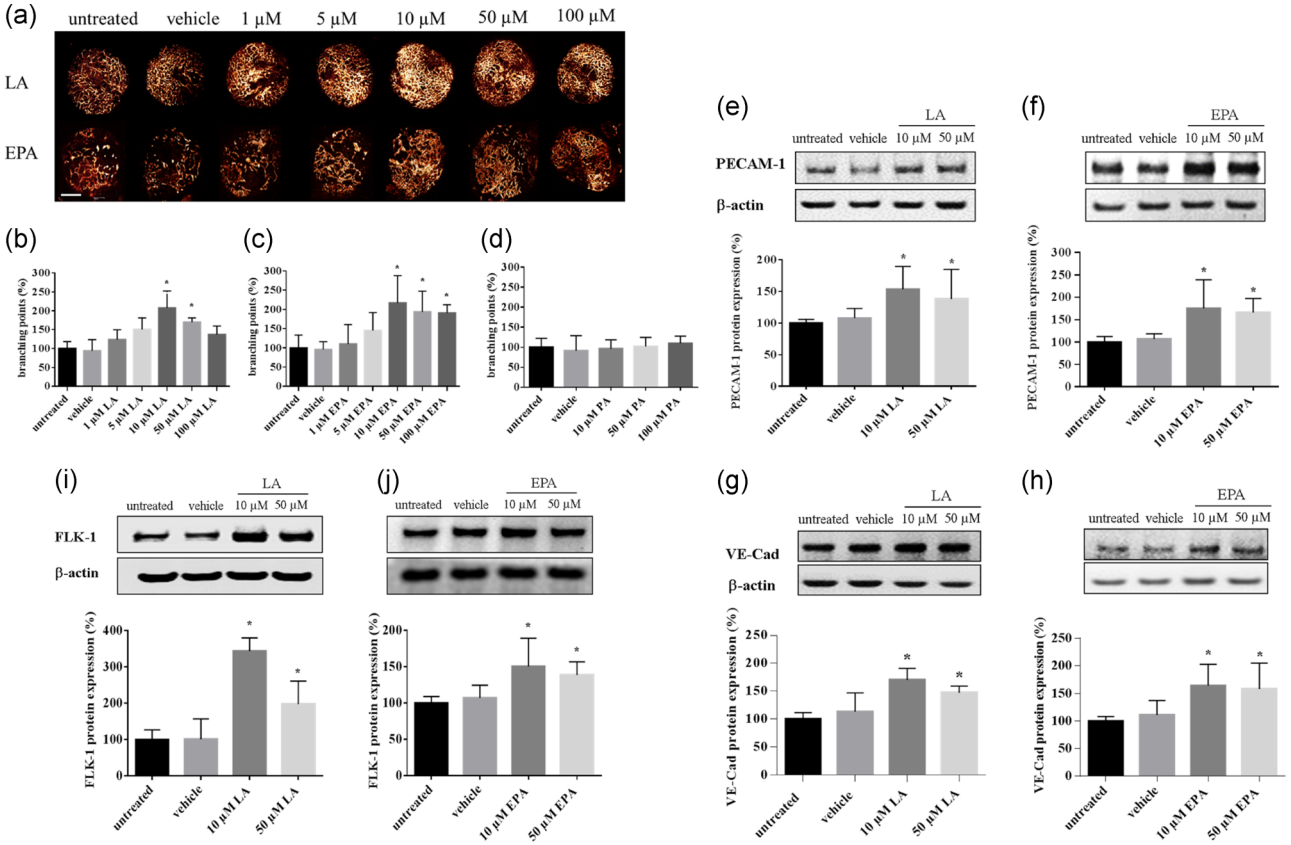

FIGURE 1 Stimulation of vasculogenesis and vascular marker expression by EPA and LA. ES cells differentiating within embryoid bodies were treated from Day 3 to 10 of cell culture with increasing concentrations (1–100 μM) of either EPA or LA, remained untreated or were treated with vehicle (dimethyl sulfoxide [DMSO]). Vascular structures were stained with an anti-PECAM-1 antibody and branching points were analyzed by computer-assisted image analysis. (a) Representative PECAM-1 labeled embryoid bodies. The bar represents 300 μm. (b–d) Quantitative presentation of branching points (%) following incubation with different concentrations of (b) LA ($n = 3$), (c) EPA ($n = 6$) or (d) palmitic acid (PA; $n = 3$). (e and f) Western blot analysis of PECAM-1 expression upon treatment with either (e) 10 or 50 μM LA ($n = 9$) or (f) EPA ($n = 7$). (g and h) Western blot analysis of VE-Cadherin expression upon treatment with either (g) 10 or 50 μM LA ($n = 4$) or (h) EPA ($n = 7$). (i and j) Western blot analysis of fetal liver kinase-1 (FLK-1) expression upon treatment with either (i) 10 or 50 μM LA ($n = 4$) or (j) EPA ($n = 6$). *$p < .05$, significantly different to the vehicle and control. EPA, eicosapentaenoic acid; ES, embryonic stem; LA, linoleic acid; PECAM-1, platelet endothelial cell adhesion molecule-1

calcium chelator BAPTA-AM (10 μM) completely abolished the calcium response observed with PUFAs, indicating that calcium was released from intracellular stores (Figures 4aiv,x). CD36 imports fatty acids inside cells and is a member of the class B scavenger receptor family of cell surface proteins (Glatz & Luiken, 2018). Since PUFA entry via CD36 may initiate the intracellular calcium response, we investigated whether the CD36 inhibitor sulfo-N-succinimidyl oleate (SSO; 200 μM) would affect PUFA-induced calcium transients. Indeed, the increase in intracellular calcium was associated to PUFA entry into the cell via CD36 since the calcium response was significantly reduced by SSO (Figures 4aiii,ix). When cells were pre-incubated for 24 hr with a blocking antibody against CD36 (cat. no. ABIN343926; Antikörper online), the calcium response was decreased in amplitude at an antibody concentration of 2 μg/ml (Figures 4av,xi) and totally abolished at 3 μg/ml (Figures 4avi,xii). Moreover, the intracellular calcium response upon PUFA treatment was necessary for the vasculogenesis process since pre-incubation with BAPTA-AM significantly inhibited vascular structure formation following treatment of differentiating ES cells with either EPA (50 μM) or LA (50 μM; Figure 4b,c).

3.4 | Activation of AMPK-α and PPAR-α upon PUFA treatment of ES cells

PUFAs regulate energy metabolism as ligands of PPARs. The transcription factor PPAR-α is essential for metabolic adaptation to starvation by inducing genes for β-oxidation and ketogenesis (Nakamura, Yudell, & Loor, 2014). In cooperation with AMPK, PPAR-α activates fatty acid oxidation to switch the cellular energy supply from glycolysis to fatty acid utilization (Grabacka, Pierzchalska, & Reiss, 2013). To investigate whether LA and EPA activate PPAR-α and AMPK-α, phospho-specific antibodies were applied. Indeed both LA (50 μM) and EPA (50 μM) increased phosphorylation of AMPK-α at residue Thr172, starting already 5 min after PUFA application (Figure 5a,b), whereas total protein expression remained

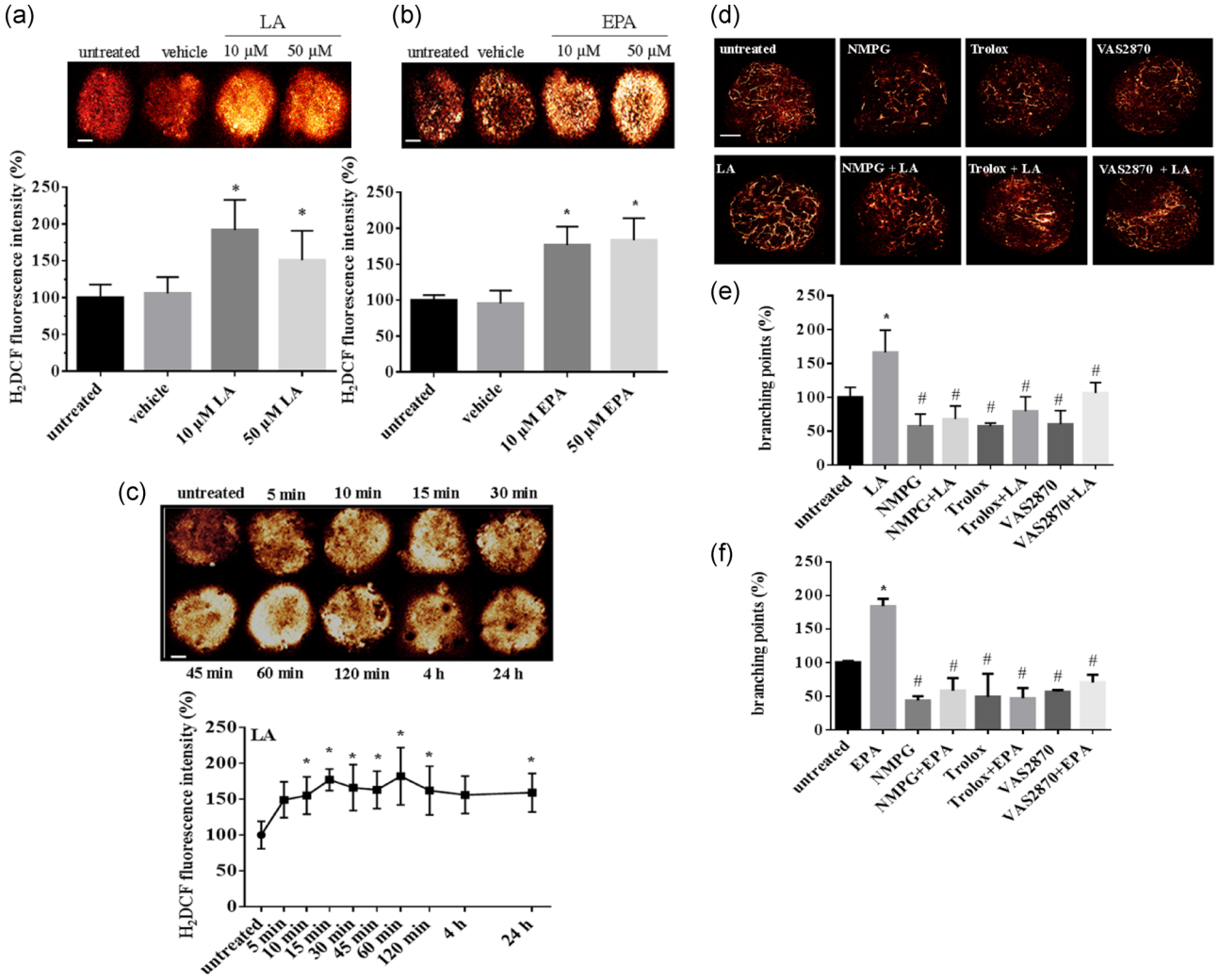

FIGURE 2 Generation of ROS in EPA as well as LA treated differentiating ES cells and effects of free radical scavengers and NADPH oxidase inhibition on vasculogenesis. (a and b) Embryoid bodies (4-day-old) were treated with either 10 or 50 μM LA (a) or EPA (b) or vehicle (DMSO) and ROS generation was assessed 24 hr thereafter using H_2DCF as fluorescent ROS indicator ($n = 3$). Shown are representative DCF-labeled embryoid bodies. The bar represents 200 μm. (c) Time course of ROS generation after different min of LA (50 μM) incubation ($n = 3$). (d–f) Effect of the free radical scavengers NMPG (100 μM) and Trolox (100 μM) or the NADPH oxidase inhibitor VAS2870 (50 μM) on vascular branch formation. (d) Representative embryoid bodies stained with an antibody against CD31. The bar represents 200 μm. (e and f) Quantitative analysis of vascular branching points (%) following treatment with (e) LA (50 μM; $n = 3$) or (f) EPA ($n = 3$). $^{*}p < .05$, significantly different to the untreated control, $^{\#}p < .05$, significantly different to the PUFA treated sample. DCF, 2′7′-dichlorofluorescein; DMSO, dimethyl sulfoxide; EPA, eicosapentaenoic acid; ES, embryonic stem; H_2DCF, 2′7′-dichlorodihydrofluorescein; LA, linoleic acid; PUFA, polyunsaturated fatty acid; ROS, reactive oxygen species

unchanged (data not shown). Moreover, activation of PPAR-α at residue S12 was observed with comparable time kinetics (Figure 5c,d). To identify the location of activated PPAR-α, cells enzymatically dissociated from 4-day-old embryoid bodies and plated on cover slips were incubated for 60 min with either EPA (50 μM) or LA (50 μM) and stained with a phospho-specific anti-PPAR-α antibody. Our date clearly showed that phospho-PPAR-α exclusively localized to cell nuclei of all cells under inspection. This effect could be abolished upon pre-incubation (2 hr) with the PPAR-α inhibitor GW6471 (5 μM) which drives the displacement of co-activators from PPAR-α and promotes the recruitment of co-repressor proteins like nuclear co-repressor (Xu et al., 2002; Figure 5e,f).

3.5 | Effect of calcium chelation as well as NADPH oxidase and eNOS inhibition on AMPK-α activation upon PUFA treatment of ES cells

The data of the present study demonstrate that treatment of differentiating ES cell with ω-3 and ω-6 PUFAs raised intracellular calcium, ROS and NO. To investigate whether the observed activation of AMPK-α is related to these intracellular messengers, experiments were carried out, where NADPH oxidase was inhibited with VAS2870 (50 μM), intracellular calcium was chelated with BAPTA-AM (10 μM) and eNOS was inhibited with L-NAME (100 μM). Our data demonstrate that inhibition of NADPH oxidase by VAS2870 totally abolished AMPK-α activation by LA (50 μM; Figure 6a). Moreover, AMPK-α activation by

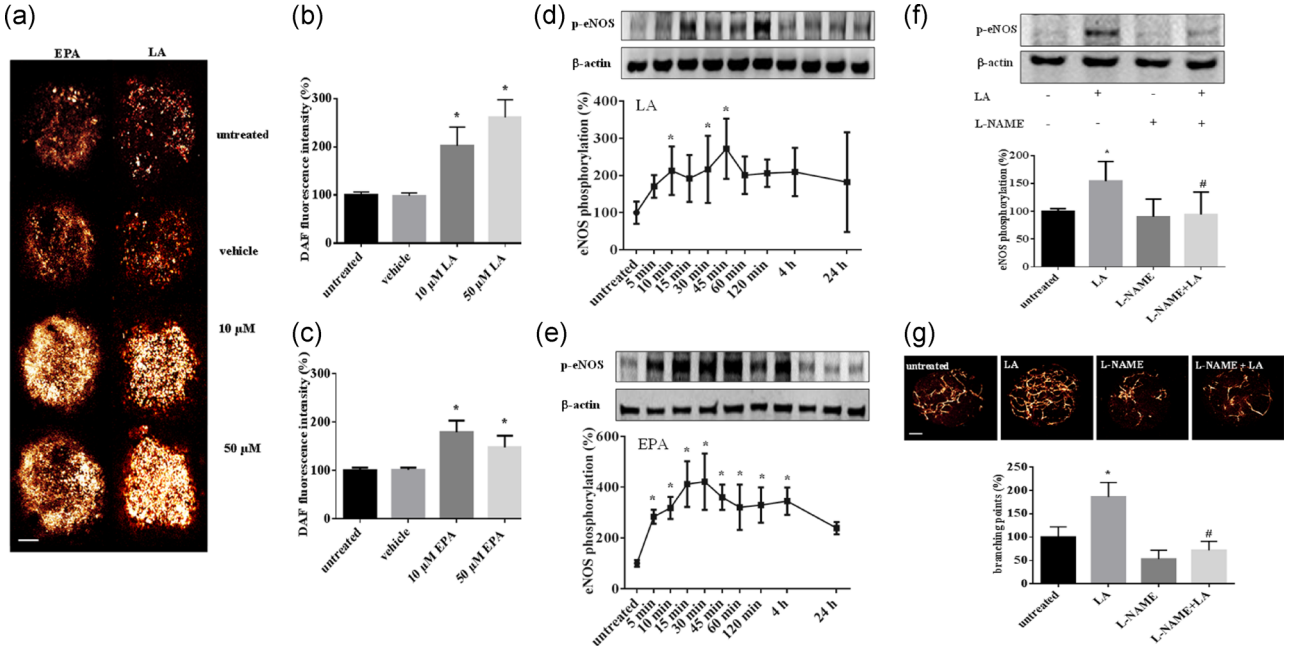

FIGURE 3 Generation of NO in EPA as well as LA treated differentiating ES cells and effect of the NOS inhibitor L-NAME on vasculogenesis. (a–c) Embryoid bodies (4-day-old) were treated with either (a and b) 10 or 50 µM LA or (a and c) EPA or vehicle (DMSO) and NO generation was assessed 24 hr thereafter using DAF-FM as fluorescent NO indicator. In (a) representative embryoid bodies labeled with DAF-FM are shown which were treated with either 10 or 50 µM EPA and LA, respectively. The bar represents 200 µm. (b and c) Quantification of DAF fluorescence (%) following treatment with (b) LA ($n = 3$) and (c) EPA ($n = 4$). (d and e) Western blot analysis of eNOS phosphorylation at different time points of (d) LA (50 µM; $n = 6$) and (e) EPA (50 µM; $n = 3$) application. (f) Effect of the NOS inhibitor L-NAME on eNOS phosphorylation following treatment of embryoid bodies with LA (50 µM) as evaluated by western blot analysis ($n = 6$). (g) Effect of L-NAME on vasculogenesis (PECAM-1 staining) elicited upon treatment of differentiating ES cells with LA (50 µM; $n = 3$). $^{*}p < .05$, significantly different to the untreated control, $^{\#}p < .05$, significantly different to the PUFA treated sample. DAF, diaminofluorescein; DMSO, dimethyl sulfoxide; eNOS, endothelial NO synthase; EPA, eicosapentaenoic acid; ES, embryonic stem; LA, linoleic acid; NO, nitric oxide; PECAM-1, platelet endothelial cell adhesion molecule-1; PUFA, polyunsaturated fatty acid

LA (50 µM) and EPA (50 µM) was inhibited upon pre-incubation with L-NAME (Figure 6d,e) as well as with BAPTA (Figure 6b,c).

3.6 | Abrogation of PUFA-mediated vasculogenesis upon inhibition of PPAR-α

If PUFAs are stimulating vasculogenesis of ES cells via AMPK-α and downstream of PPAR-α, inhibition of the latter should abolish this effect. To validate our assumption we performed experiments, where differentiating ES cells were co-incubated with the PPAR-α inhibitor GW6471. Our data demonstrate that upon co-incubation of EPA (50 µM) and LA (50 µM) with GW6471 (5 µM) the stimulation of vasculogenesis, as evaluated by assessment of vascular branching points, was completely abolished (Figure 6f,g). This finding clearly underscores the impact of PPAR-α for PUFA-induced vasculogenesis of ES cells (see Figure 7).

4 | DISCUSSION

In the present study, the effects of EPA as a lead substance for ω-3 and LA for ω-6 PUFAs were investigated. It was demonstrated that EPA as well as LA stimulated vasculogenesis in a comparable concentration range, that is, between 1 and 100 µM and maximum effects at 10 and 50 µM. Previously reported range of physiological concentrations of EPA and LA in human serum amount to 14–100 µM and 2,270–3,850 µM, respectively (Dumancas, Purdie & Reilly, L, 2010). Interestingly the saturated fatty acid PA did not show any effect on vasculogenesis of ES cells, suggesting that the unsaturated double bond chemical structure of fatty acids may be a decisive determinant for their biological function. Moreover, this finding supports the notion, that dietary intake of PUFAs may support vasculogenesis and vascular health in comparison to saturated fatty acids like PA.

EPA and LA treatment increased ROS as well as NO generation, which was abolished in presence of the NADPH oxidase inhibitor VAS2870 and the NOS inhibitor L-NAME. Moreover, PUFA-stimulated vasculogenesis was blunted upon inhibition of ROS and NO generation by using pharmacologic NADPH oxidase and eNOS inhibitors. These data corroborate previous studies of us showing that the stimulation of vasculogenesis in ES cells by arachidonic acid was dependent on ROS generation (Huang, Sharifpanah, Becker, Wartenberg, & Sauer, 2016). It is well reported that upon chemical reaction of ROS with NO, peroxynitrite is formed which—in high concentrations—is generally regarded as very reactive and toxic substance and causes endothelial dysfunction (Kanaan & Harper, 2017). In low, physiologic, concentrations, ROS/reactive nitrogen species (ROS/RNS) species including hydrogen peroxide,

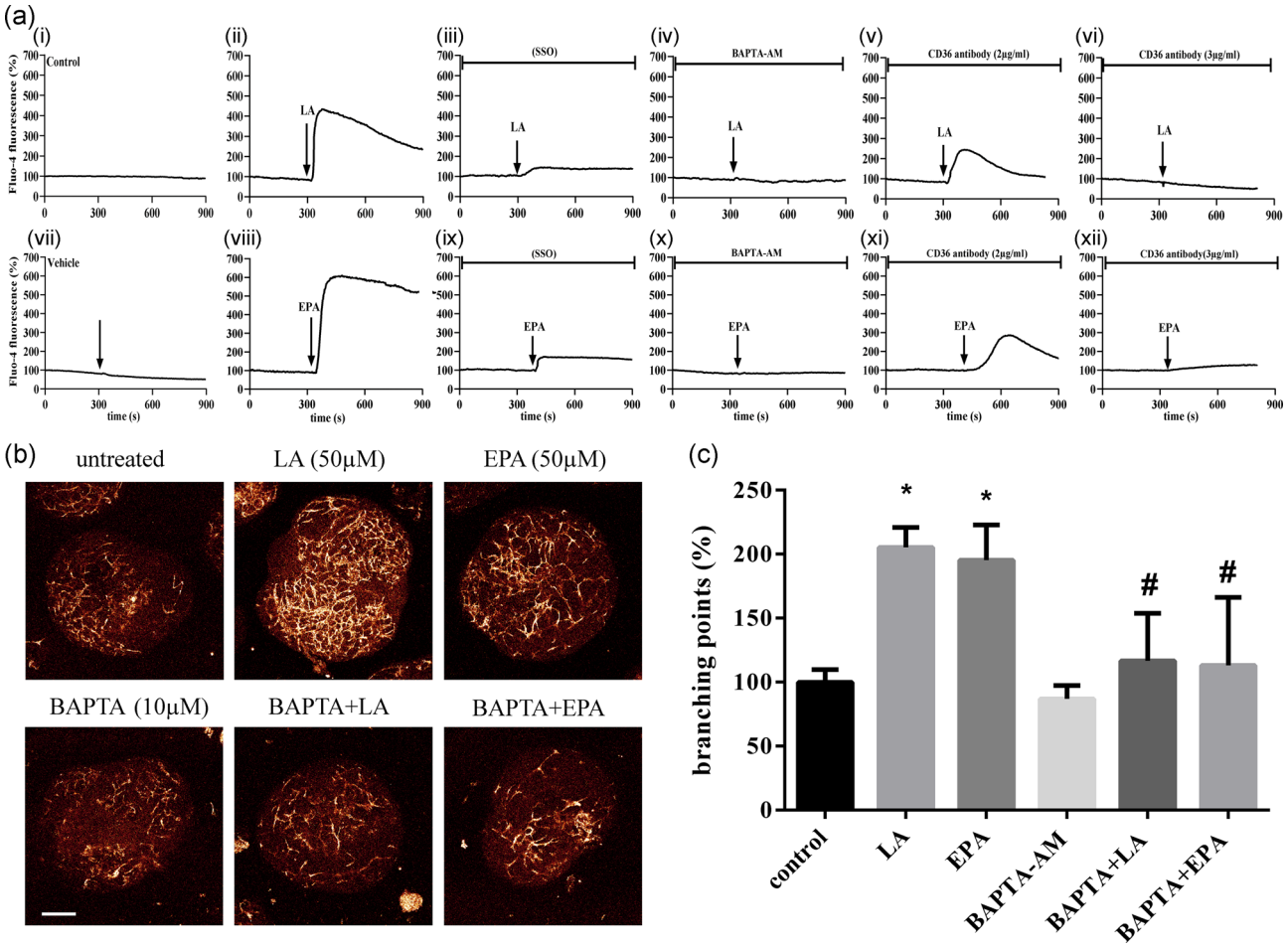

FIGURE 4 Release of intracellular calcium upon treatment of differentiating ES cells with EPA and LA. Intracellular calcium was monitored by Fluo-4 microfluorometry in single cells enzymatically dissociated from 3-day-old embryoid bodies. (ai) control ($n = 4$), (avii) vehicle (DMSO; $n = 3$), (aii) LA (50 μM; $n = 3$), (aviii) EPA (50 μM; $n = 3$), (aiii) LA (50 μM) in presence of SSO (200 μM; $n = 3$), (aix) EPA (50 μM) in presence of SSO (200 μM; $n = 3$), (aiv) LA (50 μM) in presence of BAPTA-AM (10 μM; $n = 3$), (ax) EPA (50 μM) in presence of BAPTA-AM (10 μM; $n = 3$), (av) LA (50 μM), (axi) EPA (50 μM) in presence of CD36 antibody (2 μg/ml; $n = 3$), (avi) LA (50 μM), (axii) EPA (50 μM) in the presence of CD36 antibody (3 μg/ml; $n = 3$). (b and c) Inhibition of PUFA-induced vasculogenesis by intracellular calcium chelation. Embryoid bodies were treated from Day 3 to 10 of differentiation with either EPA (50 μM) or LA (50 μM) either in absence of presence of BAPTA-AM (10 μM). Vascular structures were visualized by PECAM-1 immunostaining. In (b) representative embryoid bodies labeled with an antibody against PECAM-1 are shown. The bar represents 200 μm. The quantitative data on vascular branch formation (branching points [%]) (c) were assessed by computer-assisted image analysis of PECAM-1 positive vascular structures ($n = 3$). $^{*}p < .05$, significantly different to the untreated control, $^{\#}p < .05$, significantly different to the PUFA treated sample. EPA, eicosapentaenoic acid; ES, embryonic stem; LA, linoleic acid; PECAM-1, platelet endothelial cell adhesion molecule-1; PUFA, polyunsaturated fatty acid; SSO, sulfo-N-succinimidyl oleate

superoxide, and peroxynitrite are second messenger molecules, which are involved in functional oxidative and nitrosative modification of proteins (Hansen et al., 2016; Sauer, Wartenberg, & Hescheler, 2001). In this respect, previous studies have demonstrated that ROS and NO are critical determinants in cardiovascular differentiation of stem cells (Bekhite et al., 2016; Gentile, Muise-Helmericks, & Drake, 2013; Huang, Fleissner, Sun, & Cooke, 2010; Sharifpanah et al., 2015; Sharifpanah et al., 2016). Notably, peroxynitrite in low physiologic concentrations may be proangiogenic and act as intracellular messenger. This has been evidenced in studies, where peroxynitrite increased vascular endothelial growth factor (VEGF) expression in vascular endothelial cells (Platt et al., 2005), mediated VEGF-dependent angiogenic function in brain microvascular endothelial cells by c-src and MT1-matrix metalloproteinase activation (Prakash et al., 2012), and stimulated cell endothelial cell migration by focal adhesion kinase activation as well as low molecular weight protein tyrosine phosphatase S-glutathionylation (Abdelsaid & El-Remessy, 2012).

It is well known that ω-3 and ω-6 PUFAs are metabolized in distinct intracellular pathways. AA is the substrate for the series 2 prostaglandins, prostacyclins, thromboxanes, and leukotrienes (LTB4, series B4 LT); EPA is the substrate for the series 3 prostanoids and LTB5 (series B5 LT; Benatti, Peluso, Nicolai, & Calvani, 2004). The redox biology of PUFAs is complex and not sufficiently investigated. Generally, it is assumed that ω-3 PUFAs are anti-oxidative and anti-inflammatory, whereas ω-6 PUFAs exert pro-oxidative and pro-inflammatory effects (Sokola-Wysoczanska et al., 2018). However,

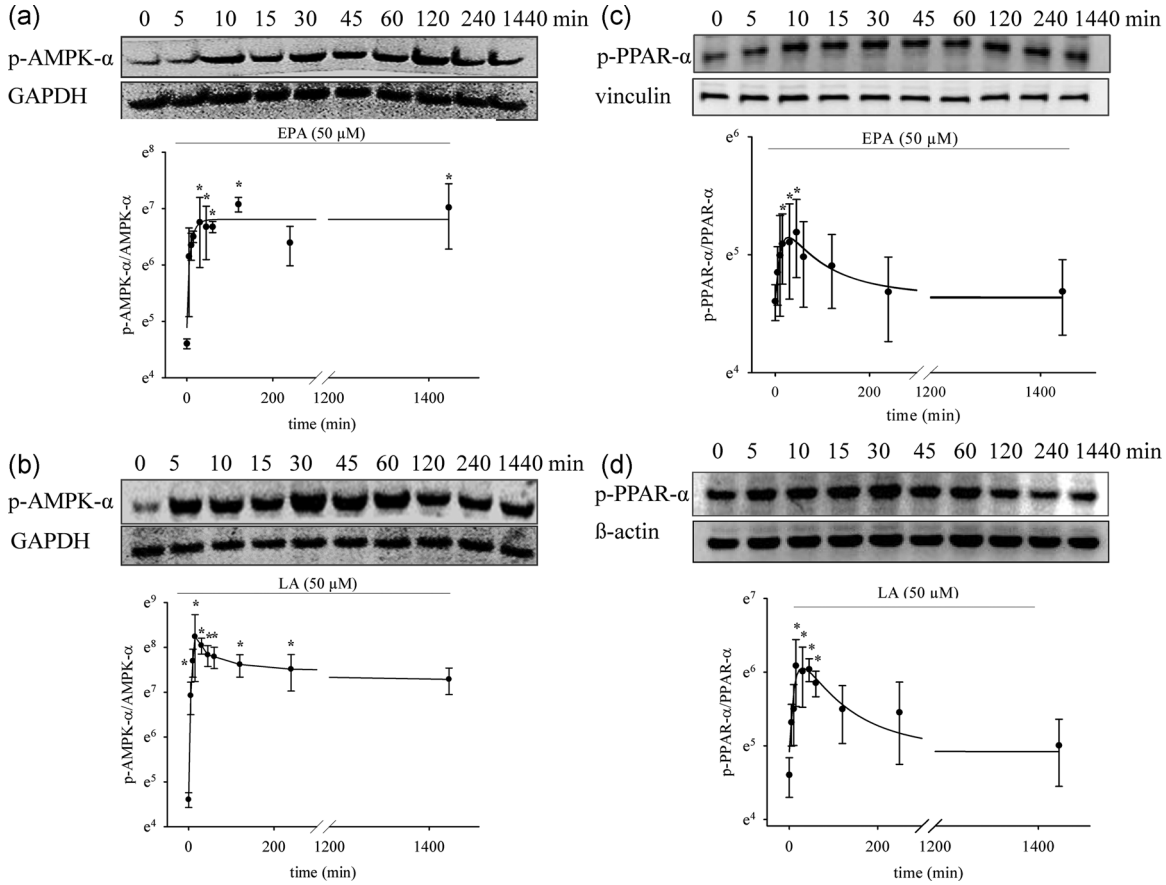

FIGURE 5 Time course of AMPK-α and PPAR-α activation upon treatment of differentiating ES cells with PUFAs. Five-day-old EBs were treated with 50 µM of either EPA or LA and protein was collected at different time points and subjected to western blot analysis. (a and b) AMPK-α phosphorylation following treatment with either (a) EPA or (b) LA. The upper panels show representative western blots stained with a phospho-specific antibody against AMPK-α. The lower panels show the means + *SD* of (n = 4) experiments for EPA and LA, respectively, corrected for total AMPK-α protein expression (p-AMPK-α/AMPK-α). (c and d) PPAR-α phosphorylation following treatment with either EPA (c) or LA (d). The upper panels show representative western blots stained with a phospho-specific antibody against PPAR-α. The lower panels show the means + *SD* of (n = 10) experiments for EPA and (n = 8) for LA, respectively, corrected for total PPAR-α protein expression (p-PPAR-α/PPAR-α). $^{*}p < .05$, significantly different to time 0 min. (e and f) Nuclear PPAR-α activation in single cells enzymatically dissociated from 3-day-old embryoid bodies upon treatment for 1 hr with either LA (50 µM) or EPA (50 µM) or pretreatment (2 hr) with GW6471 (5 µM). (e) Representative cells which were labeled with a phospho-specific antibody against PPAR-α (upper row) or only secondary antibody (2. Ab), co-stained with the nuclear cell marker DRAQ5 (middle row) and merged (lower row). The bar represents 15 µm. (f) Bar chart showing the means ± *SD* of nuclear p-PPAR-α expression upon PUFA treatment in absence and presence of GW6471 (5 µM; n = 3) $^{*}p < .05$, significantly different to the untreated control, $^{\#}p < .05$, significantly different to the PUFA treated sample. AMPK, AMP activated protein kinase-α; EPA, eicosapentaenoic acid; ES, embryonic stem; LA, linoleic acid; PPAR-α, peroxisome proliferator-activated receptor-α; PUFA, polyunsaturated fatty acid; *SD*, standard deviation

this notion was recently challenged since a number of studies reported that also ω-3 PUFAs moderately raise ROS in several cell types like endothelial cells (Okada et al., 2017), vascular smooth muscle (Crnkovic et al., 2012) and skeletal smooth muscle cells (da Silva, Nachbar, Levada-Pires, Hirabara, & Lambertucci, 2016). Interestingly ROS arising from PUFAs have been frequently noticed in tumor cells, for example, colon cancer cells (Pettersen et al., 2016) as well as lung and melanoma cancer cells (Zajdel, Wilczok, & Tarkowski, 2015; Zajdel, Wilczok, Chodurek, Gruchlik, & Dzierzewicz, 2013). This is of importance since aggressive cancer cells mimic early-development stem cells and properties of ES cells are retained in cancer cells (Ratajczak, Bujko, Mack, Kucia, & Ratajczak, 2018).

The intracellular signaling cascade resulting in ROS/RNS generation is not sufficiently investigated. The initial step should be the uptake of PUFAs into the cell. The cellular import of PUFAs is accomplished by CD36, which is a member of the class B scavenger receptor family of cell surface proteins. Inside the cell PUFAs may elicit intracellular calcium responses. This has been shown for LA in pancreatic β cells (Zhao et al., 2013), bovine neutrophils (Mena et al., 2013), HeLa cells (Figueroa et al., 2013), and mouse ES cells (Kim, Kim, Kim, Kim, & Han, 2009). EPA raised intracellular calcium in several cell types including endothelial cells (Kim et al., 2015; Okuda et al., 1994; Omura et al., 2001; Wu et al., 2018), human colon epithelial cells (Kim et al., 2015) and vascular smooth muscle cells (Engler, Ma, & Engler, 1999).

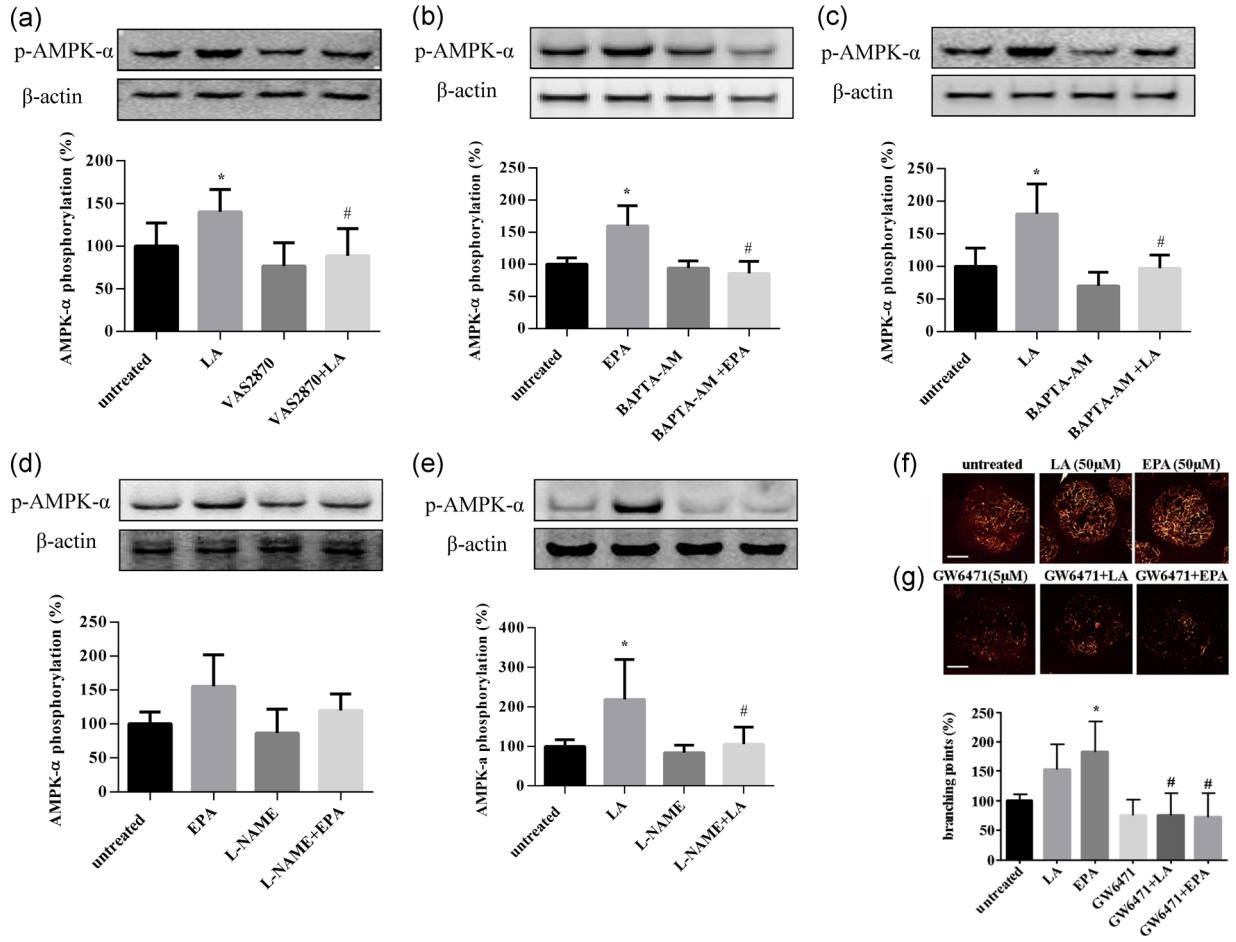

FIGURE 6 Inhibition of PUFA-induced AMPK-α activation by interference with calcium, ROS and NO signaling. Five-day-old embryoid bodies were treated with 50 μM of either EPA or LA and protein was collected 30 min thereafter and subjected to western blot analysis. Pretreatment with VAS2870 (50 μM), BAPTA-AM (10 μM), L-NAME (100 μM), and GW6471 (5 μM) was done 2 hr before addition of PUFAs. (a) LA-induced AMPK-α activation was abolished by the NADPH oxidase inhibitor VAS2870 ($n = 7$). (b and d) EPA, and (c and e) LA-induced AMPK-α activation was abolished by the NOS inhibitor L-NAME ($n = 3$ for EPA and $n = 5$ for LA) and the calcium chelator BAPTA-AM ($n = 4$ for EPA and LA, respectively). Shown are representative western blots as well as bar charts showing the means + *SD* of the indicated number of experiments. (f and g) Inhibition of PUFA-induced vasculogenesis by the PPAR-α inhibitor GW6471. The images in (f) show representative embryoid bodies treated from Day 3 to 10 of differentiation with PUFAs, either in absence or presence of GW6471 (the bar represents 200 μm). The bar chart in (g) shows the means + *SD* of $n = 6$ experiments. $^{*}p < .05$, significantly different to the untreated control, $^{\#}p < .05$, significantly different to the PUFA treated sample. AMPK, AMP activated protein kinase-α; EPA, eicosapentaenoic acid; LA, linoleic acid; NO, nitric oxide; NOS, NO synthase; PPAR-α, peroxisome proliferator-activated receptor-α; PUFA, polyunsaturated fatty acid; ROS, reactive oxygen species; *SD*, standard deviation

Intracellular calcium responses elicited by EPA in endothelial cells and smooth muscle cells were independent of NO generation (Okuda et al., 1997), which may indicate that the calcium response is upstream of NO generation. Calcium dependence of eNOS is well documented in the scientific literature (Vanhoutte, Zhao, Xu, & Leung, 2016). In the present study EPA as well as LA transiently raised intracellular calcium which was totally inhibited upon pre-incubation with the calcium chelator BAPTA-AM and significantly reduced by the CD36 inhibitor SSO as well as by a blocking antibody against CD36, suggesting that PUFAs enter cells via CD36 and release calcium from intracellular stores. The intracellular calcium response is apparently a prerequisite for ROS generation since BAPTA-AM abolished the effect. Moreover, ROS/NO are necessary for the vasculogenic effects of PUFAs since the NADPH oxidase inhibitor VAS2870 as well as the NOS inhibitor L-NAME abolished the differentiation of blood vessel-like structures upon PUFA treatment.

PUFAs have been previously shown to activate the metabolic sensor AMPK, which senses ATP deficiency and blocks anabolic processes (Shackelford & Shaw, 2009). Upon activation, AMPK inhibits glycolysis by phosphorylation of multiple forms of phosphofructo-2-kinase and by mammalian target of rapamycin inhibition, and in parallel initiates energy supply in form of fatty acid oxidation (Grabacka et al., 2013). The activity of AMPK is upstream of PPAR-α which is responsible for fat mobilization during fasting and activates mitochondrial and peroxisomal fatty acid β- and ω-oxidation and ketogenesis, simultaneously inhibiting glycolysis and fatty acid

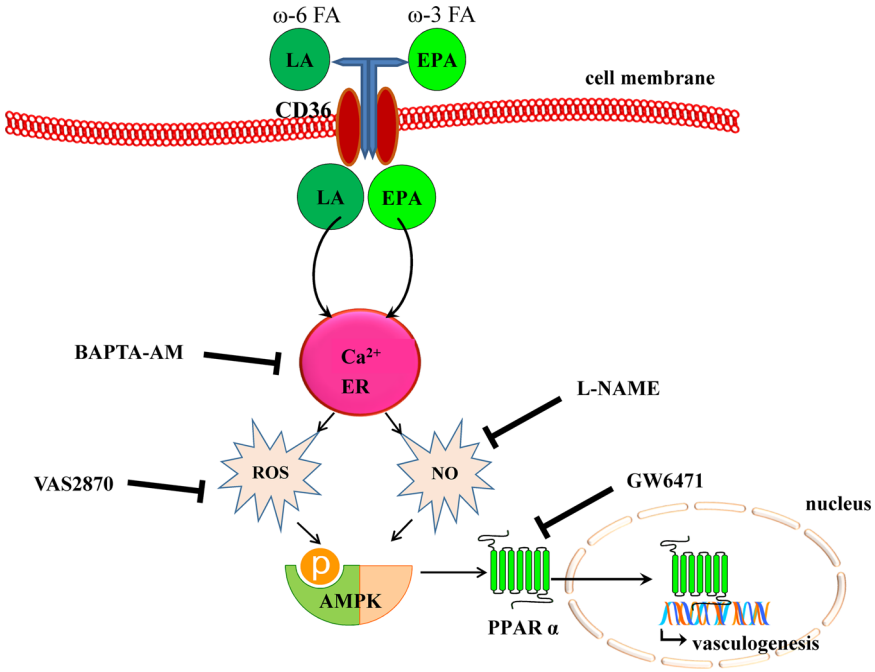

FIGURE 7 Schematic view of the stimulation of vasculogenesis in ES cells by PUFAs. LA and EPA are entering the cell through CD36 and release intracellular calcium from intracellular stores. Calcium stimulates ROS from NADPH oxidase and NO from eNOS, which in concert activate AMPK. Downstream of AMPK, PPAR-α is phosphorylated in the cell nucleus and initiates vasculogenic genes. AMPK, AMP activated protein kinase; eNOS, endothelial NO synthase; EPA, eicosapentaenoic acid; ES, embryonic stem; LA, linoleic acid; NO, nitric oxide; PPAR-α, peroxisome proliferator-activated receptor-α; PUFA, polyunsaturated fatty acid; ROS, reactive oxygen species

synthesis (Grabacka et al., 2013). The data of the present study show that EPA as well as LA activated AMPK-α and PPAR-α. Previous studies have evidenced that ω-3 PUFAs increased fatty acid oxidation in AMPK-dependent manner to generate ATP, thereby inhibiting unnecessary pathways, such as fatty acid synthesis (Lyons & Roche, 2018). Our data show that AMPK-α activation was dependent on PUFA-induced intracellular calcium, ROS and NO changes, since activation was abolished upon calcium chelation as well as inhibition of NADPH oxidase and NOS. This is in line with previous studies of us, demonstrating that PPAR-α agonists, such as WY14,643, GW7647, and ciprofibrate stimulated cardiomyogenesis of ES cells by a mechanism involving ROS generation (Sharifpanah, Wartenberg, Hannig, Piper, & Sauer, 2008). Consequently, the PPAR-α inhibitor GW6471 inhibited vasculogenesis elicited by EPA and LA in the present study.

Stem cell pluripotency does not represent a single defined metabolic state. Metabolic signatures are highly characteristic for a cell and may contribute to the fate of the cell (Ellen Kreipke, Wang, Miklas, Mathieu, & Ruohola-Baker, 2016). Cellular metabolism is changing between naïve (early stage) and primed (late stage) ES cells, representing preimplantation and postimplantation embryos, respectively. The transition from naïve to primed ES cells has been shown to be accompanied by a distinct metabolic switch from bivalent (fatty acid oxidation/glycolytic) to highly glycolytic state which adopts the cells to the hypoxic condition of the early postimplantation embryo and protects the embryo from oxidative stress (Ellen Kreipke et al., 2016). During the following differentiation and maturation processes a second metabolic switch towards oxidative phosphorylation occurs. Then highly respiring mitochondria fulfill the dramatically augmenting energy needs during shaping of the cardiovascular system and organ formation. This physiological "metabolic inflammation" requires ROS/RNS as well as PUFA-derived eicosanoids as intracellular messengers to initiate differentiation and maturation of progenitor cells in the cardiovascular system.

ACKNOWLEDGMENT

This work was supported by a grant from the RB Bretzel Foundation and a scholarship to Amer Taha from the German Academic Exchange Service (DAAD).

CONFLICT OF INTERESTS

The authors declare that there are no conflict of interests.

AUTHOR CONTRIBUTIONS

A. T. and F. S. performed the experiments. M. W. and H. S. designed and drafted the present study.

DATA AVAILABILITY STATEMENT

The data that support the findings of this study are available from the corresponding author, (H. S.), upon reasonable request.

ORCID

Amer Taha http://orcid.org/0000-0002-7665-0574
Fatemeh Sharifpanah http://orcid.org/0000-0001-7435-1805
Heinrich Sauer http://orcid.org/0000-0002-9144-4728

REFERENCES

Abdelhamid, A. S., Brown, T. J., Brainard, J. S., Biswas, P., Thorpe, G. C., Moore, H. J., … Hooper, L. (2018). Omega-3 fatty acids for the primary and secondary prevention of cardiovascular disease. *Cochrane Database of Systematic Reviews*, *7*. CD003177.

Abdelsaid, M. A., & El-Remessy, A. B. (2012). S-glutathionylation of LMW-PTP regulates VEGF-mediated FAK activation and endothelial cell migration. *Journal of Cell Science*, *125*(Pt 20), 4751–4760.

Ali, E. H., Sharifpanah, F., Wartenberg, M., & Sauer, H. (2018). Silibinin from *Silybum marianum* stimulates embryonic stem cell vascular differentiation via the STAT3/PI3-K/AKT axis and nitric oxide. *Planta Medica*, *84*(11), 768–778.

Bartsch, C., Bekhite, M. M., Wolheim, A., Richter, M., Ruhe, C., Wissuwa, B., … Wartenberg, M. (2011). NADPH oxidase and eNOS control cardiomyogenesis in mouse embryonic stem cells on ascorbic acid treatment. *Free Radical Biology and Medicine*, *51*(2), 432–443.

Bekhite, M. M., Muller, V., Troger, S. H., Muller, J. P., Figulla, H. R., Sauer, H., & Wartenberg, M. (2016). Involvement of phosphoinositide 3-kinase class IA (PI3K 110alpha) and NADPH oxidase 1 (NOX1) in regulation of vascular differentiation induced by vascular endothelial growth factor (VEGF) in mouse embryonic stem cells. *Cell and Tissue Research*, *364*(1), 159–174.

Benatti, P., Peluso, G., Nicolai, R., & Calvani, M. (2004). Polyunsaturated fatty acids: Biochemical, nutritional and epigenetic properties. *Journal of the American College of Nutrition*, *23*(4), 281–302.

Carrillo, C., del Mar Cavia, M., & Alonso-Torre, S.R. (2011). Oleic acid versus linoleic and α-linolenic acid. Different effects on Ca2+ signaling in rat thymocytes. *Cell Physiol Biochem*, *27*(3-4), 373–380.

Cencioni, C., Spallotta, F., Savoia, M., Kuenne, C., Guenther, S., Re, A., … Gaetano, C. (2018). Zeb1-Hdac2-eNOS circuitry identifies early cardiovascular precursors in naive mouse embryonic stem cells. *Nature Communications*, *9*(1), 1281.

Cha, Y., Han, M. J., Cha, H. J., Zoldan, J., Burkart, A., Jung, J. H., … Kim, K. S. (2017). Metabolic control of primed human pluripotent stem cell fate and function by the miR-200c-SIRT2 axis. *Nature Cell Biology*, *19*(5), 445–456.

Chantzichristos, V. G., Agouridis, A. P., Moutzouri, E., Stellos, K., Elisaf, M. S., & Tselepis, A. D. (2016). Effect of rosuvastatin or its combination with omega-3 fatty acids on circulating CD34(+) progenitor cells and on endothelial colony formation in patients with mixed dyslipidaemia. *Atherosclerosis*, *251*, 240–247.

Crnkovic, S., Riederer, M., Lechleitner, M., Hallstrom, S., Malli, R., Graier, W. F., … Frank, S. (2012). Docosahexaenoic acid-induced unfolded protein response, cell cycle arrest, and apoptosis in vascular smooth muscle cells are triggered by Ca(2)(+)-dependent induction of oxidative stress. *Free Radical Biology and Medicine*, *52*(9), 1786–1795.

da Silva, E. P., Jr., Nachbar, R. T., Levada-Pires, A. C., Hirabara, S. M., & Lambertucci, R. H. (2016). Omega-3 fatty acids differentially modulate enzymatic anti-oxidant systems in skeletal muscle cells. *Cell Stress and Chaperones*, *21*(1), 87–95.

Dumancas, G. G. K., Purdie, M., & Reilly, L. N. (2010). Partial least squares (PLS1) algorithm for quantitating cholesterol and polyunsaturated fatty acids in human serum. *Journal of Biotech Research*, *2*, 121–130.

Ellen Kreipke, R., Wang, Y., Miklas, J. W., Mathieu, J., & Ruohola-Baker, H. (2016). Metabolic remodeling in early development and cardiomyocyte maturation. *Seminars in Cell and Developmental Biology*, *52*, 84–92.

Engler, M. B., Ma, Y. H., & Engler, M. M. (1999). Calcium-mediated mechanisms of eicosapentaenoic acid-induced relaxation in hypertensive rat aorta. *American Journal of Hypertension*, *12*(12 Pt 1-2), 1225–1235.

Figueroa, V., Saez, P. J., Salas, J. D., Salas, D., Jara, O., Martinez, A. D., … Retamal, M. A. (2013). Linoleic acid induces opening of connexin26 hemichannels through a PI3K/Akt/Ca(2+)-dependent pathway. *Biochimica et Biophysica Acta/General Subjects*, *1828*(3), 1169–1179.

Gentile, C., Muise-Helmericks, R. C., & Drake, C. J. (2013). VEGF-mediated phosphorylation of eNOS regulates angioblast and embryonic endothelial cell proliferation. *Developmental Biology*, *373*(1), 163–175.

Glatz, J. F. C., & Luiken, J. (2018). Dynamic role of the transmembrane glycoprotein CD36 (SR-B2) in cellular fatty acid uptake and utilization. *Journal of Lipid Research*, *59*(7), 1084–1093.

Grabacka, M., Pierzchalska, M., & Reiss, K. (2013). Peroxisome proliferator activated receptor alpha ligands as anticancer drugs targeting mitochondrial metabolism. *Current Pharmaceutical Biotechnology*, *14*(3), 342–356.

Hansen, T., Galougahi, K. K., Celermajer, D., Rasko, N., Tang, O., Bubb, K. J., & Figtree, G. (2016). Oxidative and nitrosative signalling in pulmonary arterial hypertension—Implications for development of novel therapies. *Pharmacology and Therapeutics*, *165*, 50–62.

Hu, J., Fromel, T., & Fleming, I. (2018). Angiogenesis and vascular stability in eicosanoids and cancer. *Cancer and Metastasis Reviews*, *37*(2-3), 425–438.

Huang, N. F., Fleissner, F., Sun, J., & Cooke, J. P. (2010). Role of nitric oxide signaling in endothelial differentiation of embryonic stem cells. *Stem Cells and Development*, *19*(10), 1617–1626.

Huang, Y. H., Sharifpanah, F., Becker, S., Wartenberg, M., & Sauer, H. (2016). Impact of arachidonic acid and the leukotriene signaling pathway on vasculogenesis of mouse embryonic stem cells. *Cells Tissues Organs*, *201*(5), 319–332.

Innes, J. K., & Calder, P. C. (2018). Omega-6 fatty acids and inflammation. *Prostaglandins Leukotrienes and Essential Fatty Acids*, *132*, 41–48.

Kanaan, G. N., & Harper, M. E. (2017). Cellular redox dysfunction in the development of cardiovascular diseases. *Biochimica et Biophysica Acta, General Subjects*, *1861*(11 Pt A), 2822–2829.

Kanayasu, T., Morita, I., Nakao-Hayashi, J., Asuwa, N., Fujisawa, C., Ishii, T., … Murota, S. (1991). Eicosapentaenoic acid inhibits tube formation of vascular endothelial cells in vitro. *Lipids*, *26*(4), 271–276.

Kang, J. X., & Liu, A. (2013). The role of the tissue omega-6/omega-3 fatty acid ratio in regulating tumor angiogenesis. *Cancer and Metastasis Reviews*, *32*(1-2), 201–210.

Kim, J. M., Lee, K. P., Park, S. J., Kang, S., Huang, J., Lee, J. M., … Im, D. S. (2015). Omega-3 fatty acids induce Ca(2+) mobilization responses in human colon epithelial cell lines endogenously expressing FFA4. *Acta Pharmacologica Sinica*, *36*(7), 813–820.

Kim, M. H., Kim, M. O., Kim, Y. H., Kim, J. S., & Han, H. J. (2009). Linoleic acid induces mouse embryonic stem cell proliferation via Ca2+/PKC, PI3K/Akt, and MAPKs. *Cellular Physiology and Biochemistry*, *23*(1-3), 53–64.

Lyons, C. L., & Roche, H. M. (2018). Nutritional Modulation of AMPK-Impact upon Metabolic-Inflammation. *International Journal of Molecular Sciences*, *19*(10), 3092.

Mascheck, L., Sharifpanah, F., Tsang, S. Y., Wartenberg, M., & Sauer, H. (2015). Stimulation of cardiomyogenesis from mouse embryonic stem cells by nuclear translocation of cardiotrophin-1. *International Journal of Cardiology*, *193*, 23–33.

Mathew, S. A., & Bhonde, R. R. (2018). Omega-3 polyunsaturated fatty acids promote angiogenesis in placenta derived mesenchymal stromal cells. *Pharmacological Research*, *132*, 90–98.

Mena, J., Manosalva, C., Ramirez, R., Chandia, L., Carroza, D., Loaiza, A., … Hidalgo, M. A. (2013). Linoleic acid increases adhesion, chemotaxis, granule release, intracellular calcium mobilisation, MAPK phosphorylation, and gene expression in bovine neutrophils. *Veterinary Immunology and Immunopathology*, *151*(3-4), 275–284.

Mobraten, K., Haug, T. M., Kleiveland, C. M., & Tor, L. (2013). Omega-3 and omega-6 PUFAs induce the same GPR120-mediated signalling events, but with different kinetics and intensity in Caco-2 cells. *Lipids Health Disease*, *12*, 101.

Morishita, T., Uzui, H., Ikeda, H., Amaya, N., Kaseno, K., Ishida, K., … Tada, H. (2016). Association of CD34/CD133/VEGFR2-positive cell numbers with eicosapentaenoic acid and postprandial hyperglycemia in patients

with coronary artery disease. *International Journal of Cardiology*, *221*, 1039–1042.

Nakamura, M. T., Yudell, B. E., & Loor, J. J. (2014). Regulation of energy metabolism by long-chain fatty acids. *Progress in Lipid Research*, *53*, 124–144.

Okada, T., Morino, K., Nakagawa, F., Tawa, M., Kondo, K., Sekine, O., … Maegawa, H. (2017). N-3 polyunsaturated fatty acids decrease the protein expression of soluble epoxide hydrolase via oxidative stress-induced P38 kinase in rat endothelial cells. *Nutrients*, *9*(7), 654.

Okuda, Y., Ezure, M., Tsukahara, K., Sawada, T., Mizutani, M., Katori, T., … Yamashita, K. (1994). Eicosapentaenoic acid enhances intracellular free calcium in cultured human endothelial cells. *Biochemical Medicine and Metabolic Biology*, *51*(2), 166–168.

Okuda, Y., Kawashima, K., Sawada, T., Tsurumaru, K., Asano, M., Suzuki, S., … Yamashita, K. (1997). Eicosapentaenoic acid enhances nitric oxide production by cultured human endothelial cells. *Biochemical and Biophysical Research Communications*, *232*(2), 487–491.

Omura, M., Kobayashi, S., Mizukami, Y., Mogami, K., Todoroki-Ikeda, N., Miyake, T., & Matsuzaki, M. (2001). Eicosapentaenoic acid (EPA) induces Ca(2+)-independent activation and translocation of endothelial nitric oxide synthase and endothelium-dependent vasorelaxation. *FEBS Letters*, *487*(3), 361–366.

Pettersen, K., Monsen, V. T., Hakvag Pettersen, C. H., Overland, H. B., Pettersen, G., Samdal, H., … Schonberg, S. A. (2016). DHA-induced stress response in human colon cancer cells—Focus on oxidative stress and autophagy. *Free Radical Biology and Medicine*, *90*, 158–172.

Platt, D. H., Bartoli, M., El-Remessy, A. B., Al-Shabrawey, M., Lemtalsi, T., Fulton, D., & Caldwell, R. B. (2005). Peroxynitrite increases VEGF expression in vascular endothelial cells via STAT3. *Free Radical Biology and Medicine*, *39*(10), 1353–1361.

Prakash, R., Somanath, P. R., El-Remessy, A. B., Kelly-Cobbs, A., Stern, J. E., Dore-Duffy, P., … Ergul, A. (2012). Enhanced cerebral but not peripheral angiogenesis in the Goto-Kakizaki model of type 2 diabetes involves VEGF and peroxynitrite signaling. *Diabetes*, *61*(6), 1533–1542.

Ratajczak, M. Z., Bujko, K., Mack, A., Kucia, M., & Ratajczak, J. (2018). Cancer from the perspective of stem cells and misappropriated tissue regeneration mechanisms. *Leukemia*, *32*(12), 2519–2526.

Rimm, E. B., Appel, L. J., Chiuve, S. E., Djousse, L., Engler, M. B., Kris-Etherton, P. M., … Lichtenstein, A. H. American Heart Association Nutrition Committee of the Council on Lifestyle and Cardiometabolic Health; Council on Epidemiology and Prevention; Council on Cardiovascular Disease in the Young; Council on Cardiovascular and Stroke Nursing; and Council on Clinical Cardiology (2018). Seafood long-chain n-3 polyunsaturated fatty acids and cardiovascular disease: A Science Advisory From the American Heart Association. *Circulation*, *138*(1), e35–e47.

Sauer, H., Wartenberg, M., & Hescheler, J. (2001). Reactive oxygen species as intracellular messengers during cell growth and differentiation. *Cellular Physiology and Biochemistry*, *11*(4), 173–186.

Shackelford, D. B., & Shaw, R. J. (2009). The LKB1-AMPK pathway: Metabolism and growth control in tumour suppression. *Nature Reviews Cancer*, *9*(8), 563–575.

Sharifpanah, F., Ali, E. H., Wartenberg, M., & Sauer, H. (2019). The milk thistle (*Silybum marianum*) compound Silibinin stimulates leukopoiesis from mouse embryonic stem cells. *Phytotherapy Research*, *33*(2), 452–460.

Sharifpanah, F., Behr, S., Wartenberg, M., & Sauer, H. (2016). Mechanical strain stimulates vasculogenesis and expression of angiogenesis guidance molecules of embryonic stem cells through elevation of intracellular calcium, reactive oxygen species, and nitric oxide generation. *Biochimica et Biophysica Acta/General Subjects*, *1863*(12), 3096–3105.

Sharifpanah, F., De Silva, S., Bekhite, M. M., Hurtado-Oliveros, J., Preissner, K. T., Wartenberg, M., & Sauer, H. (2015). Stimulation of vasculogenesis and leukopoiesis of embryonic stem cells by extracellular transfer RNA and ribosomal RNA. *Free Radical Biology and Medicine*, *89*, 1203–1217.

Sharifpanah, F., Wartenberg, M., Hannig, M., Piper, H. M., & Sauer, H. (2008). Peroxisome proliferator-activated receptor alpha agonists enhance cardiomyogenesis of mouse ES cells by utilization of a reactive oxygen species-dependent mechanism. *Stem Cells*, *26*(1), 64–71.

Sokola-Wysoczanska, E., Wysoczanski, T., Wagner, J., Czyz, K., Bodkowski, R., Lochynski, S., & Patkowska-Sokola, B. (2018). Polyunsaturated fatty acids and their potential therapeutic role in cardiovascular system disorders-A review. *Nutrients*, *10*(10), 1561.

Spencer, L., Mann, C., Metcalfe, M., Webb, M., Pollard, C., Spencer, D., … Dennison, A. (2009). The effect of omega-3 FAs on tumour angiogenesis and their therapeutic potential. *European Journal of Cancer*, *45*(12), 2077–2086.

Tsuzuki, T., Shibata, A., Kawakami, Y., Nakagawa, K., & Miyazawa, T. (2007). Conjugated eicosapentaenoic acid inhibits vascular endothelial growth factor-induced angiogenesis by suppressing the migration of human umbilical vein endothelial cells. *Journal of Nutrition*, *137*(3), 641–646.

Turgeon, J., Dussault, S., Maingrette, F., Groleau, J., Haddad, P., Perez, G., & Rivard, A. (2013). Fish oil-enriched diet protects against ischemia by improving angiogenesis, endothelial progenitor cell function, and postnatal neovascularization. *Atherosclerosis*, *229*(2), 295–303.

Vanhoutte, P. M., Zhao, Y., Xu, A., & Leung, S. W. (2016). Thirty years of saying no: Sources, fate, actions, and misfortunes of the endothelium-derived vasodilator mediator. *Circulation Research*, *119*(2), 375–396.

Wu, K. C., Wong, K. L., Wang, M. L., Shiao, L. R., Leong, I. L., Gong, C. L., … Leung, Y. M. (2018). Eicosapentaenoic acid triggers Ca(2+) release and Ca(2+) influx in mouse cerebral cortex endothelial bEND.3 cells. *The Journal of Physiological Sciences: JPS*, *68*(1), 33–41.

Xia, S., Li, X. P., Cheng, L., Han, M. T., Zhang, M. M., Shao, Q. X., … Qi, L. (2015). Fish oil-rich diet promotes hematopoiesis and alters hematopoietic niche. *Endocrinology*, *156*(8), 2821–2830.

Xu, H. E., Stanley, T. B., Montana, V. G., Lambert, M. H., Shearer, B. G., Cobb, J. E., … Stimmel, J. B. (2002). Structural basis for antagonist-mediated recruitment of nuclear co-repressors by PPARalpha. *Nature*, *415*(6873), 813–817.

Zajdel, A., Wilczok, A., Chodurek, E., Gruchlik, A., & Dzierzewicz, Z. (2013). Polyunsaturated fatty acids inhibit melanoma cell growth in vitro. *Acta Poloniae Pharmaceutica*, *70*(2), 365–369.

Zajdel, A., Wilczok, A., & Tarkowski, M. (2015). Toxic effects of n-3 polyunsaturated fatty acids in human lung A549 cells. *Toxicology In Vitro*, *30*(1 Pt B), 486–491.

Zhao, Y., Wang, L., Qiu, J., Zha, D., Sun, Q., & Chen, C. (2013). Linoleic acid stimulates [Ca2+]i increase in rat pancreatic beta-cells through both membrane receptor- and intracellular metabolite-mediated pathways. *PLoS One*, *8*(4):e60255.

How to cite this article: Taha A, Sharifpanah F, Wartenberg M, Sauer H. Omega-3 and Omega-6 polyunsaturated fatty acids stimulate vascular differentiation of mouse embryonic stem cells. *J Cell Physiol*. 2020;235:7094–7106. https://doi.org/10.1002/jcp.29606